Influence of time lag effect between winter wheat canopy temperature and atmospheric temperature on the accuracy of CWSI inversion of photosynthetic parameters

Yujin Wang
wangyujin@nwafu.edu.cn

Northwest A&F University https://orcid.org/0009-0000-7048-7473

Yule Lu
Ning Yang
Jiankun Wang
Zugui Huang
Youzhen Xiang
Junying Chen
Zhitao Zhang

Research Article

Keywords: time lag effect, CWSI, photosynthetic parameters, machine learning

Posted Date: April 22nd, 2024

DOI: https://doi.org/10.21203/rs.3.rs-4277221/v1

Version of Record: A version of this preprint was published at Plants on June 19th, 2024. See the published version at https://doi.org/10.3390/plants13121702.

Influence of time lag effect between winter wheat canopy temperature and atmospheric temperature on the accuracy of CWSI inversion of photosynthetic parameters

Yujin Wang[a,b], Yule Lu[a,b], Ning Yang[a,b], Jiankun Wang[a,b], Zugui Huang[a,b], Youzhen Xiang[a,b], Junying Chen[a,b], Zhitao Zhang[a,b*]

[a]College of Water Resources and Architectural Engineering, Northwest A&F University, Yangling 712100, China

[b]Key Laboratory of Agricultural Soil and Water Engineering in Arid and Semiarid Areas, Ministry of Education, Northwest A&F University, Yangling 712100, China

[*]Correspondence:Zhitao Zhang

E-mail: zhitaozhang@126.com

Abstract

Aims Considering time lag effects between atmospheric temperature (Ta) and canopy temperature (Tc) may improve the accuracy of Crop Water Stress Index (CWSI) inversions of photosynthetic parameters, which is crucial for enhancing the precision in monitoring crop water stress conditions.

Methods In this study, four moisture treatments were set up, T1 (95% of field water holding capacity), T2 (80% of field water holding capacity), T3 (65% of field water holding capacity), and T4 (50% of field water holding capacity). We quantified the time-lag parameter in winter wheat using time-lag peak-seeking, time-lag cross-correlation, time-lag mutual information, and grey time-lag correlation analysis; Based on the time lag parameter, we modified CWSI theoretical and empirical model, and assessed the impact of time lag effects on the accuracy of CWSI inversion of photosynthesis parameters. Finally, we applied several machine learning algorithms to predict the daily variation of CWSI after time-lag correction.

Results The results showed that: (1) The time lag parameter calculated using the time-lag peak-seeking, time-lag cross-correlation, time-lag mutual information, and grey time-lag correlation an-alysis were 44-70, 32-44, 42-58, and 76-97 min. (2) CWSI empirical model corrected by the time-lag mutual information method had the highest correlation with photosynthetic parameters. (3) GA-SVM had the highest prediction accuracy for CWSI empirical model corrected by the time-lag mutual information method.

Conclusions Considering time lag effects between Ta and Tc effectively enhanced the correlation between CWSI and photosynthetic parameters,which can provide theoretical support for thermal infrared remote sensing to diagnose crop water stress conditions.

Keywords: time lag effect; CWSI; photosynthetic parameters; machine learning

Introduction

Timely and accurate diagnosis of crop water stress conditions effectively determines the timing of irrigation and facilitates precision irrigation, crucial for enhancing water use efficiency (WUE) and increasing yield (Kifle and Gebretsadikan 2016; Liu et al. 2016a). When crops experience water stress, their physiological indicators, such as photosynthetic parameters, leaf water potential, and external morphology, undergo changes. These changes encompass a decrease in leaf area index, a reduction in chlorophyll concentration, and a diminution in leaf length and width (Saini et al. 2024; Zhang M et al. 2023). Physiological indicators, including photosynthetic parameters, leaf water potential, and stem water potential, focus on the crop itself for research and offer a straightforward, scientific method to diagnose the status of crop water deficit. These indicators have proven effective in monitoring the water status of crops (Carrasco-Benavides et al. 2024). Moisture stress impacts photosynthetic parameters across reproductive period of crops, displaying consistent trends in net photosynthesis rate (Pn), transpiration rate (Tr), and stomatal conductance (gs), which all decrease with increasing moisture stress (Desoky et al. 2021). The extent of changes in photosynthetic parameters varies with different levels of water stress, with minor reductions under mild water stress and significant declines under moderate to severe water stress (Liu EK et al. 2016).

Beyond physiological indicators of crop water deficit, Crop Water Stress Index (CWSI), sensitive to soil moisture, stands as a reliable indirect metric for monitoring crop water status. Under water stress conditions, crops exhibit reduced stomatal conductance and diminished transpiration cooling, leading to an increase in canopy temperature. Idso et al. (1981) found that the differential in canopy temperature following noon effectively measures crop water deficit, revealing a consistent linear relationship between the canopy-air temperature differential (CTD) and vapor pressure deficit (VPD) under clear sky conditions, which is not affected by environmental factors such as wind speed.In response to the above phenomenon, Idso et al. (1981)

proposes CWSI empirical model, which has the advantages of fewer computational parameters, ease of measurement, and sensitivity to crop varieties. Jackson et al. (1981) proposed CWSI theoretical model based on the principle of canopy energy balance, taking into account environmental factors such as aerodynamic resistance, crop minimum canopy resistance, and net radiation, making CWSI model more theoretical.

CWSI is a sensitive indicator to reflect the water stress caused by stomatal function of the crop, and continuous water stress results in an increasing trend of CWSI and a decreasing trend of Pn、Tr and Gs. there is a good negative correlation between CWSI and photosynthetic parameters (R^2 = 0.94) (Desoky et al. 2021; Pipatsitee et al. 2018).

In calculating CWSI, previous researchers always used atmospheric temperature (Ta) and canopy temperature (Tc) at the same moment (Gonzalez-Dugo and Zarco-Tejada 2022). However, there is the time lag effect in the response of Tc to Ta (Huang et al. 2022). Therefore, it is more accurate to use the atmospheric temperature that actually influences the canopy temperature. (Zhang et al. 2024) discovered that accounting for the time lag effect significantly enhances the accuracy of CWSI in estimating soil water content. Currently, research on the impact of this time lag on the accuracy of CWSI in the inversion of photosynthetic parameters remains unexplored.

Given these considerations, we selected winter wheat throughout its entire reproductive period as the subject of our study. We quantified the time lag parameters between Ta and Tc using methods such as time-lag peak-seeking, time-lag cross-correlation, time-lag mutual information, and grey time-lag correlation analysis. Subsequently, we corrected CWSI theoretical and empirical model based on these time lag parameters. Finally, we examined the impact and mechanisms of time lag effect between Ta and Tc on the accuracy of CWSI in inversing photosynthetic parameters.

Materials and methods

Study site description

The experimental site is located at the Institute of Water Saving Agriculture in Arid Regions, Northwest Agriculture and Forestry University, Yangling District, Shaanxi Province, China (108°24'E, 34°20'N). This region is characterized by a warm temperate semi-humid monsoon climate, distinguished by four distinct seasons and moderate rainfall. The average annual temperature ranges from approximately 13℃ to 15℃. Rainfall predominantly occurs in July and August, driven by the southeast monsoon, with an annual average between 600 mm and 800 mm. The effect of groundwater recharge is not considered in this experiment.

Experiment design

The experimental site was 32.5 m×10.5 m and divided into 12 plots, each measuring 4 m×4 m. Protected row treatments were used to mitigate the effects of water infiltration(Fig.1). Four moisture treatments were used in the experiment to obtain generalisable results: T1 (fully irrigated), T2 (mild water stress), T3 (moderate water stress) and T4 (severe water stress). The upper irrigation limits were set at 95%, 80%, 65% and 50% of the field water holding capacity for T1, T2, T3 and T4. Each moisture treatment was replicated three times. Instruments for the continuous monitoring of canopy temperature and environmental factors were positioned above experimental plots 2, 5, 8, and 11. The cultivar used was "Genmai 68" winter wheat sown at 25 cm spacing with 30g of seed per row. The sowing date was 19 October 2022 and the harvest date was 1 June 2023. Irrigation was carried out by drip irrigation system, and the irrigation quota is detailed in Table 1. The measured volumetric soil water content was calculated by oven-drying method and the irrigation quota is calculated as follows:

$$m = H \bullet (\theta s - \theta o) \bullet p \bullet s \tag{1}$$

where m was irrigation quota (mm); H was planned wetted layer depth(m),0.4~0.5m (green-up stage),0.5~0.6m (jointing stage),0.6~0.8m(tasseling stage),0.8~1.0m(grouting period); θs was field capacity(%) ,which was the upper limit of soil moisture content; θ_0 was measured volumetric soil moisture content(%); s was trial plot size (m); p was drip irrigation wetting ratio,0.6.

Table 1 Irrigation quota of winter wheat

irrigation date	Irrigation quota(mm)			
	T1	T2	T3	T4
17/2/2023	46.7	43.9	19.2	18.2
25/2/2023	50.3	23.8	23.0	16.0
5/3/2023	63.0	28.5	13.4	31.2
12/3/2023	58.1	19.4	17.7	51.0
19/3/2023	64.0	54.6	40.0	16.3
29/3/2023	64.0	44.8	33.0	16.3
7/4/2023	90.3	36.0	15.8	38.0
18/4/2023	91.9	44.9	40.6	42.0
28/4/2023	29.5	25.2	19.4	17.0
12/5/2023	53.8	69.0	88.4	14.0
23/5/2023	53.9	65.0	30.6	17.9

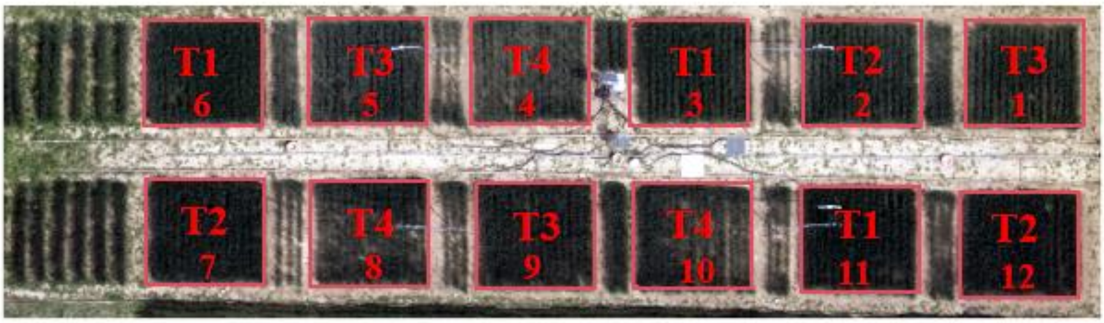

Fig. 1 Overview of the experimental site

Data acquisition

Tc measurements

In this study, the canopy temperature of winter wheat was continuously monitored using an SI-411 infrared thermometer. The monitoring interval was set at 2 minutes. Considering the effect of crop cover on the instrumental monitoring of canopy temperature, the time lag parameter was calculated in this experiment starting from 16 February 2023. The canopy temperature of winter wheat for the four moisture treatments was shown in Fig. 2.

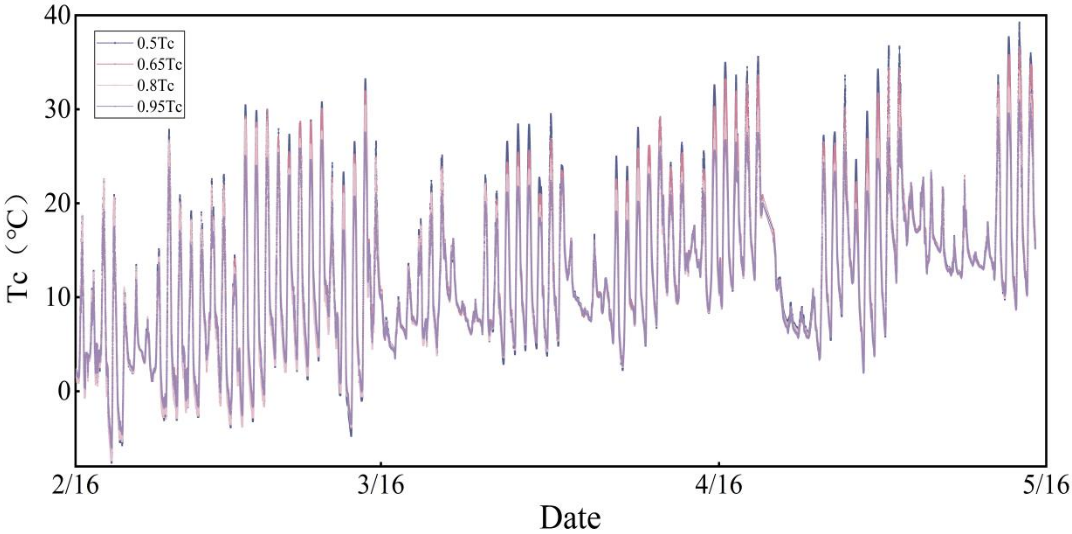

Fig. 2 Canopy temperature of winter wheat

Environmental factors measurements

In this experiment, meteorological factors were continuously monitored using the AWS-CR1000 scientific-grade automatic meteorological monitoring system, as detailed in Table 2. Data collection intervals were set at 2 minutes.

Table 2 Summary of environmental factors observed by the weather station

Variables	Sensor number	Instrument height(m)	Abbreviation	Unit
Solar radiatio	SN-500	3.5	Rs	$W\cdot m^{-2}$
Soil heat fux	HFP01	-0.10	G	$W\cdot m^{-2}$

Atmospheric temperature	HC2AS3	2.5	Ta	℃
Relative humidity	HC2AS3	2.5	RH	%
Wind speed	HC2AS3	2	u	$m \cdot s^{-1}$

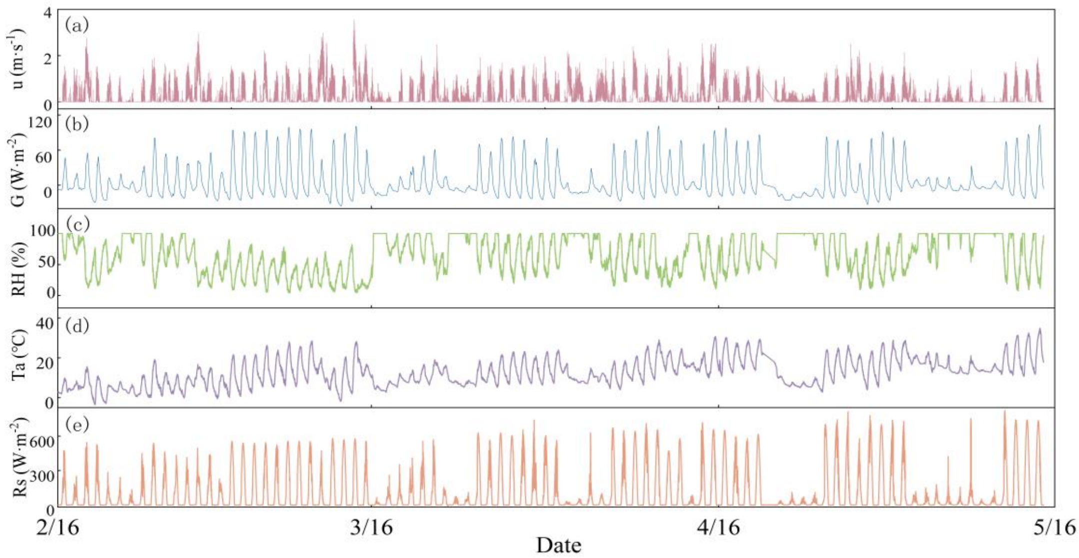

Fig. 3 Dynamic variation of (a) u($m \cdot s^{-1}$); (b) G($W \cdot m^{-2}$); (c)RH(%); (d)Ta(℃); (e)Rs($W \cdot m^{-2}$)

Photosynthetic parameters measurements

The differences in crop physiological indicators at different irrigation levels were small in the morning and evening, and the differences were largest around midday, which could accurately reflect the crop water status (Hatfield 1983; Maai et al. 2020). Therefore, we chose sunny and windless days to collect the photosynthetic parameters of winter wheat: stomatal conductance gs (mol/($m^2 \cdot s$)), net photosynthesis rate Pn (μmol/m^2), and transpiration rate Tr (mmol/($m^2 \cdot s$)) at 14:00 using a portable photosynthesizer model Li-6800 from LICOR, USA. Three wheat plants were randomly selected from each plot, and the measurements were repeated three times for each wheat flag leaf, and the average value was taken as the photosynthetic parameters of the crop under the moisture treatment; to ensure the accuracy of the acquired data, the CO_2 concentration of the Li-6800 portable photosynthesizer reached 400 μmol/mol, and the intensity of the light reached 1000 μmol/($m^2 \cdot s$)

during the measurement. The data of photosynthetic parameters were collected 12 times in this experiment (Fig. 4).

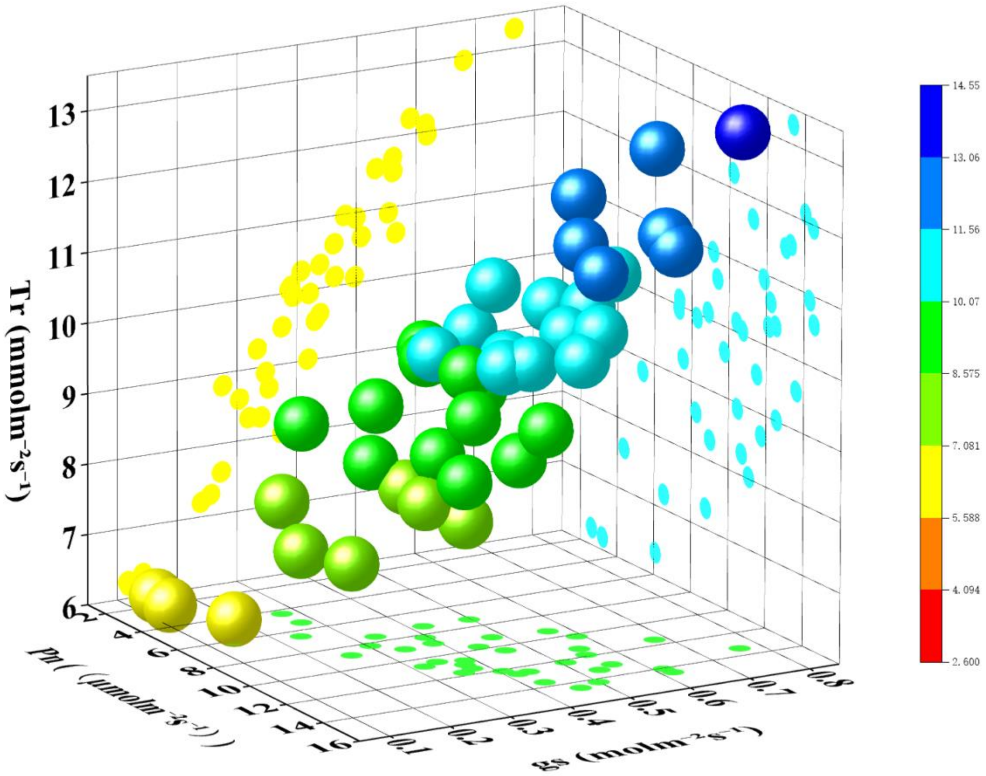

Fig. 4 Photosynthetic parameters of winter wheat

Data processing

Savitzky–Golay (S-G) filter

Savitzky-Golay (S-G) filter (Liu YP et al. 2016) is a smoothing filtering technique that employs local least squares to eliminate noise from time series data. This method achieves its smoothing effect by fitting a polynomial to the data, which effectively removes noise while preserving the signal's original shape as closely as possible. Consequently, the S-G filter maintains the integrity of the signal, ensuring effective smoothing.

Z-Score normalization

Employing the Z-Score standardization method (Guo et al. 2022), dimensionless standardization of raw indicator data effectively mitigates the impact of discrepancies in data size, characteristics, and distribution. This approach eliminates unit differences across the data, enabling comparability among variables with diverse characteristics, while preserving the original distribution pattern of the data.

Time-lag peak-seeking method

Time-lag peak-seeking method (Feng et al. 2023; Zeng et al. 2023) is to select the appropriate function to fit Ta and Tc and determine the peak position of the fitted curve. The time difference corresponding to this peak point represents the time lag parameter between Ta and Tc. CCE equation has a higher fitting accuracy for the canopy temperature after smoothing by S-G filtering, and ECS equation has a higher fitting accuracy for the atmospheric temperature after smoothing by S-G filtering.

CCE equation is expressed as follows:

$$double1\ z = x - xc_1 \tag{2}$$

$$\begin{aligned} y = y_0 + A*(\exp(-z*z/(2*w)) + (1-0.5*(1-\tan(k_2*(x-xc_2))))*\\ B*\exp(-0.5*k_3*(abs(x-xc_3)+(x-xc_3)))) \end{aligned} \tag{3}$$

where xc1 is the peak moment of winter wheat canopy temperature. The fitting accuracy was judged by the coefficient of determination (R^2).

ECS equation is expressed as follows:

$$\begin{aligned} y = y0 + A/(w*sqrt(2*pi))*(exp(-0.5*((x-xc)/w)^2)*(1+(a3/(3*2*1))*((x-xc)/w)*(((x-xc)/w)^2-3)+\\ (a_4/(4*3*2*1))*(((x-xc)/w)^4-6*((x-xc)/w)^3+3)+((10*a_3^2)/(6*5*4*3*2*1))*(((x-xc)/w)^6-\\ 15*((x-xc)/w)^4+45*((x-xc)/w)^2-15))) \end{aligned} \tag{4}$$

where xc is the moment of peak atmospheric temperature.The accuracy of the fit is judged by the coefficient of determination (R^2), and the peak time difference between Tc and Ta temperatures is the time lag parameter *between Tc and Ta.*

Time-lag cross-correlation method

X (Tc) is first mapped to Y (Ta) in the chronological order of observations. Then, Tc is shifted in steps of 2 min and the Pearson correlation coefficients of the two series are calculated. When the Pearson's correlation coefficient attains its maximum value, the corresponding shift duration is designated as the time lag parameter for the two series (Huang et al. 2022; Konda et al. 1996). Where the correlation coefficient is calculated as:

$$\mathrm{R}_k = \frac{\sum_{i=1}^{n-k}(xi - \overline{xi})(y_{i+k} - \overline{y_{i+k}})}{\sqrt{\sum_{i=1}^{n-k}(x_i - \overline{x_i})^2}\sqrt{\sum_{i=1}^{n-k}(y_{i+k} - \overline{y_{i+k}})^2}} \tag{5}$$

$$R_m = \max(R_k) \tag{6}$$

$$\mathrm{T}_L = 2m \tag{7}$$

where R_k is Pearson's correlation coefficient for a sliding shift number of K;n is sample size; x_i is canopy temperature(°C); y_{i+k} is atmospheric temperature(°C); $\overline{x_i}$ is mean of canopy temperature series(°C); $\overline{y}_{i+k}$ is mean of atmospheric temperature series(°C); R_m is maximum correlation coefficien; m is the sliding shifts in the canopy temperature series that correspond to the maximum Pearson correlation coefficient.; k=0,±1,±2,...,±n , k>0 indicates canopy temperature change ahead of atmospheric temperature, k<0 indicates that canopy temperature changes lag behind atmospheric temperature.$\mathrm{T_L}$ is time lag parameter(min).

Time-lag mutual information method

Employing the time-lag mutual information method, the time-lag parameter between canopy temperature X and atmospheric temperature Y is determined (Ji et al. 2021). The formula is presented as follows:

$$\mathrm{I}(X, Y, \tau) = \sum_{x}\sum_{y} p(x_t, y_{t+\tau}) \log \frac{p(x_t, y_{t+\tau})}{p(x_t,)p(y_{t+\tau})} \tag{8}$$

where $\mathrm{P}(x_t, y_{t+\tau})$ is $\mathrm{X = x_t, Y = y_{t+\tau}}$ joint distribution probability. τ is time lag parameter. The time lag parameter τ is determined when the mutual information coefficient reaches its peak. A positive τ means that x changes before y, while negative τ indicates that x changes after y.

Grey time-lag correlation analysis

①The reference sequence canopy temperature (Tc) is

$$\mathrm{X} = (x(1), x(2), \ldots, x(n)) \tag{9}$$

Comparison of the sequence group atmospheric temperature (Ta) is

$$Y\tau = (y(1+\tau), y(2+\tau), \ldots, y(n+\tau)) \tag{10}$$

where τ is the time lag parameter.

②Calculate the correlation coefficient $\zeta(x(k), y\tau(k+\tau))$ between X and Yτ with the following formula:

$$\zeta(x(k), y_\tau(k+\tau)) = \frac{\min\tau \min k \left|x(k) - y_\tau(k+\tau)\right| + \rho \max\tau \max k \left|x(k) - y_\tau(k+\tau)\right|}{\left|x(k) - y_\tau(k+\tau)\right| + \rho \max\tau \max k \left|x(k) - y_\tau(k+\tau)\right|} \tag{11}$$

$$k = 1, 2, 3, \ldots, n \tag{12}$$

$$\tau = 0, 1, \ldots, T - n \tag{13}$$

$$\gamma(\tau) = \frac{1}{n} \sum_{k=1}^{n} \zeta(x(k), y_\tau(k+\tau)) \tag{14}$$

$$\tau = 0, 1, \ldots, T - n \tag{15}$$

where ρ is the resolution factor, ρ = 0.5; T is the time span of the time series.

③

$$\gamma(\tau^*) = \max{}_{0 \le \tau \le T-n}\gamma(\tau) \tag{16}$$

Where $\gamma(\tau^*)$ is the grey correlation between X and Y， τ^* is the time lag parameter of Y and X.

CWSI theoretical model

Based on the canopy energy balance theory, Jackson et al. (1981) developed a theoretical model of CWSI. The formula is as follows:

$$\mathrm{CWSI}=\frac{\gamma(1+{r_c}/{r_a})-\gamma^*}{\Delta+\gamma(1+{r_c}/{r_a})} \tag{17}$$

$$\gamma=0.665\times101.3\times(\frac{293-0.0065Z}{293})^{5.26} \tag{18}$$

$$\gamma^*=\gamma\times(1+{r_c}/{r_a}) \tag{19}$$

$$\Delta=45.03+3.014\mathrm{T}+0.05345\mathrm{T}^2+0.00224\mathrm{T}^3 \tag{20}$$

$$\mathrm{T}=\frac{\mathrm{Tc}+\mathrm{T}a}{2} \tag{21}$$

$$r_a=\frac{4.72[\ln(\frac{z-d}{z_0})]^2}{(1+0.54u)} \tag{22}$$

where CWSI is crop water stress index; γ is psychrometric coefficient（Pa·°C^{-1}）; r_c is canopy resistance (s·m^{-1}); r_a is aerodynamics resistance (s·m^{-1}); Δ is slope of the water vapour pressure curve（Pa·°C^{-1}）; Z is height above sea level(m); d is zero-plane displacement(m), d=0.63h; z_0 is roughness(m), z_0=0.13h; h is crop height(m); u is reference height wind speed (m·s^{-1}); z is reference height(m), z=2; r_c is canopy resistance (s·m^{-1}), displayed in Table 3.

Table3 (Yuan et al. 2002) rc of winter wheat at different fertility stages

growth period	rc($s \cdot m^{-1}$)
regreening stage~jointing stage	13.01
jointing stage~tasseling stage	18.03
tasseling stage~filling stage	26.85

CWSI empirical model

CWSI empirical model was first constructed by Idso et al. (1981).The formula is as follows:

$$\mathrm{CWSI} = \frac{(Tc - Ta) - NWSB}{NTB - NWSB} \tag{22}$$

$$\mathrm{CTD} = \mathrm{Tc} - \mathrm{Ta} \tag{23}$$

$$\mathrm{VPD} = 0.6108 \times \exp\left(\frac{17.27 \times \mathrm{Ta}}{Ta + 237.7}\right) \times \left(\frac{100 - RH}{100}\right) \tag{24}$$

$$\mathrm{VPG} = 0.6108 \times \exp\left(\frac{17.27 \times \mathrm{Ta}}{\mathrm{Ta} \times 237.7}\right) - 0.6108 \times \exp\left(\frac{17.27 \times (\mathrm{Ta} + b)}{(\mathrm{Ta} + \mathrm{b}) + 237.7}\right) \tag{25}$$

$$\mathrm{NWSB} = a \times VPD + b \tag{26}$$

$$\mathrm{NTB} = a \times \mathrm{VPG} + b \tag{27}$$

where Tc is canopy temperature(℃); Ta is atmospheric temperature(℃); NWSB is lower bound(no water stress); NTB is upper bound(no transpiration); CTD is canopy-air temperature differential(℃);a, b are the slope and intercept of CTD and VPD linear fits;

Solar radiation intensifies during the period from 13:00 to 15:00, when the discrepancy between crop and soil water supply conditions becomes more pronounced, and the linear relationship between Canopy Temperature Difference (CTD) and Vapor Pressure Deficit (VPD) distincts (Gontia and Tiwari 2008). Consequently, this study opts for linear fitting of CTD and VPD specifically for the 13:00-15:00 interval. The results are presented in Fig 5.

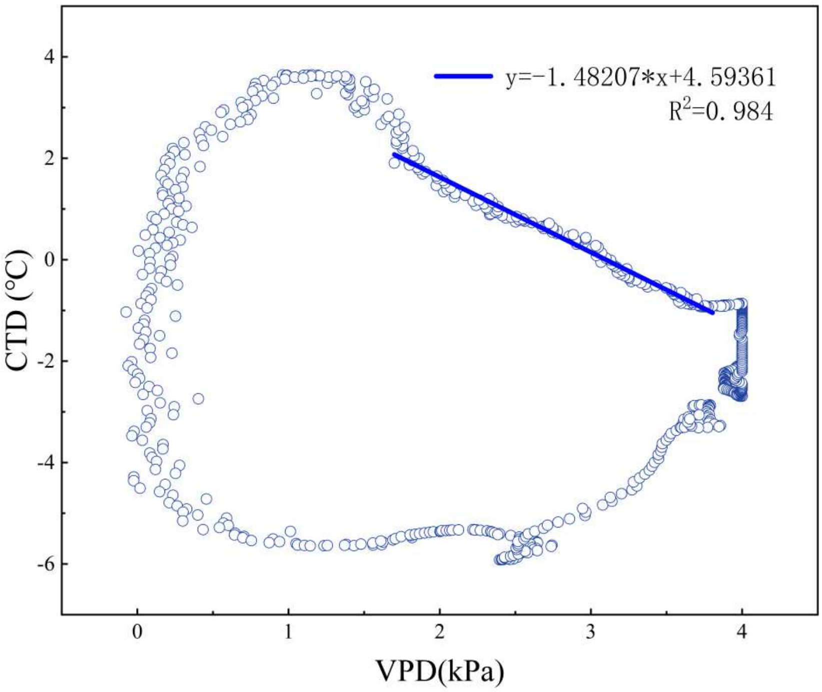

Fig. 5 Linear fit plot of VPD and CTD

Evaluation indicators

In this study, the accuracy of CWSI inversion of photosynthetic parameters, both before and after time-lag correction, is assessed using the coefficient of determination (R^2). R^2 value closer to 1 indicates higher inversion accuracy.

Similarly, the prediction accuracy of the machine learning algorithm is evaluated through the coefficient of determination (R^2) and the root-mean-square error (RMSE), with R^2 values nearing 1 and RMSE values approaching 0 denoting enhanced prediction accuracy.

Results

Time-lag parameters of winter wheat under different water stresses

As depicted in Fig. 6, the CCE equation fitted the daily variation process of winter wheat canopy temperature smoothed by S-G filtering with excellent accuracy (R^2=0.98), and the ECS equation fitted the daily variation process of atmospheric temperature smoothed by S-G filtering with equal precision (R^2=0.98). As seen in Figs. 7 through 11, among the time-lagged parameters of Tc and Ta obtained by different methods, the grey time-lag correlation analysis was the largest. The time-lag peak-seeking method and the time-lag mutual information method were the second largest, followed by the time-lag cross-correlation method.

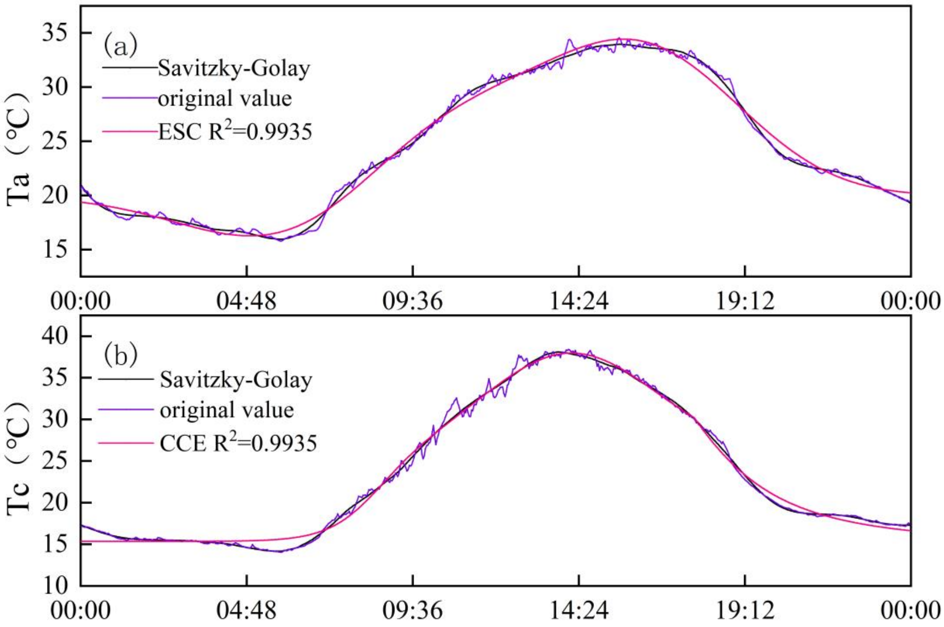

Fig. 6 (a) ESC equations fitted to S-G filter smoothed Ta (b) CCE equation fitted to S-G filter smoothed Tc

Furthermore, the time lag parameter of canopy temperature (Tc) and atmospheric temperature (Ta), calculated using the time-lag peak-finding method, time-lag cross-correlation method, time-lag mutual information method, and grey time-lag correlation analysis, were approximately 53min, 44min, 58 min, and 97 min, respectively, under T1 treatment. Under T2 treatment, these time lag parameters were about 52min, 43min 55min, and 92 min. For the T3 treatment, the time lag parameters were approximately 55 min, 44 min, 54 min, and 98 min. Lastly, under T4 treatment, the parameters were around 44 min, 32 min, 42 min, and 76 min.

This indicated that the time lag between Tc and Ta obtained from different calculation methods for T1, T2, and T3 treatment did not differ significantly, and Tc reached its peak time later for T4 treatment, resulting in a decrease in the time lag parameter between Ta and Tc by approximately 10 ~ 22 min. This phenomenon might be associated with the soil moisture threshold (Ma et al. 2018). When the soil moisture threshold was reached, the water lost through transpiration in winter wheat could not be replenished promptly. To ensure the normal life activities of the crop, the expansion rate of the crop leaves was reduced, stomatal conductance decreased significantly, transpiration rate declined, and canopy temperature continued to increase, reaching the peak time later. This led to a shorter time lag between atmospheric temperature and canopy temperature (Farooq et al. 2010).

In addition, the number of cross-correlation, mutual information coefficient, and grey correlation coefficient corresponding to the peak moments of T1, T2, T3, and T4 treatments did not differ significantly. This indicated that the linear correlation (Cao et al. 2022), nonlinear correlation (Su et al. 2008), and curve similarity (Wang et al. 2017) of Tc and Ta under the four moisture treatments after time-lag correction did not differ much.

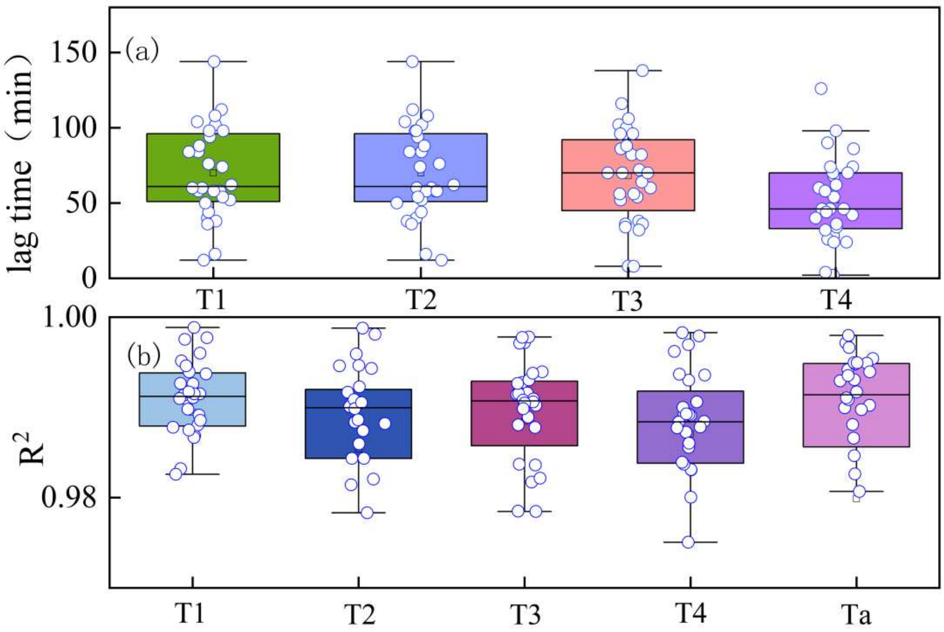

Fig. 7 (a)Time lag parameters of T1, T2, T3 and T4 calculated by time-lag peak-finding method (b)Coefficient of determination(R^2) for T1, T2, T3 and T4 fitted by the time-lag peak-finding method

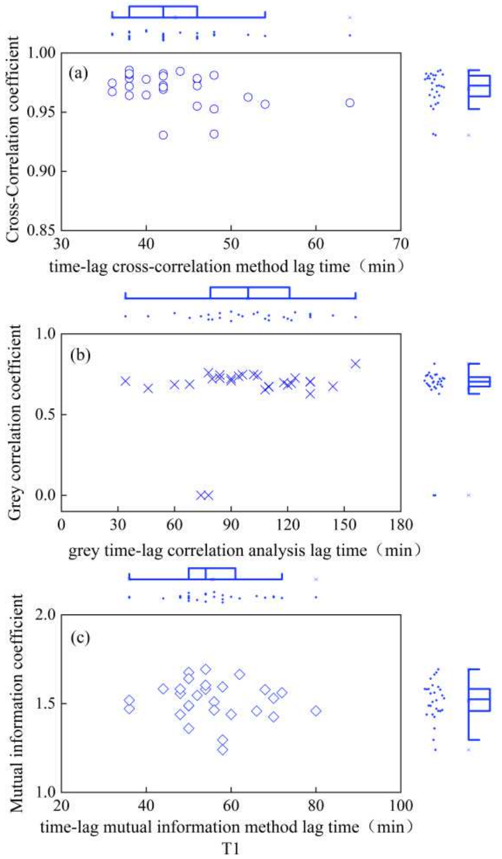

Fig. 8 Time lag parameter and corresponding coefficients for T1 calculated by time-lag cross-correlation method,time-lag mutual information method, and grey time-lag correlation analysis

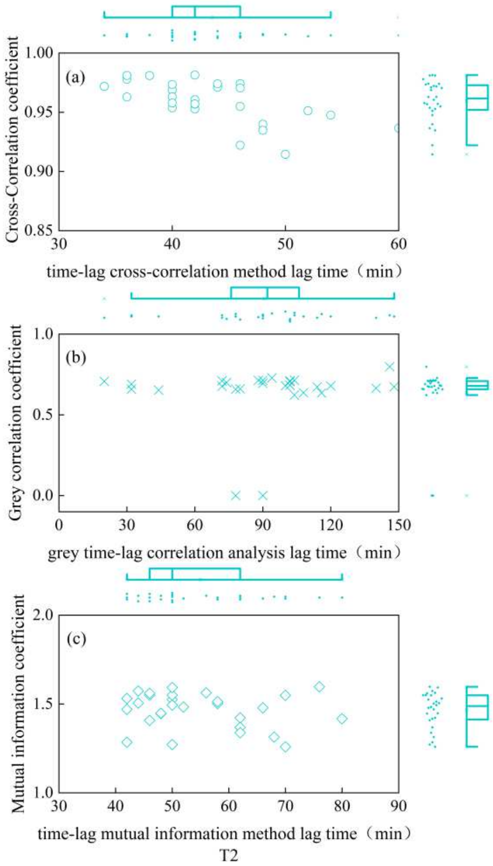

Fig. 9 Time lag parameter and corresponding coefficients for T2 calculated by time-lag cross-correlation method,time-lag mutual information method, and grey time-lag correlation analysis

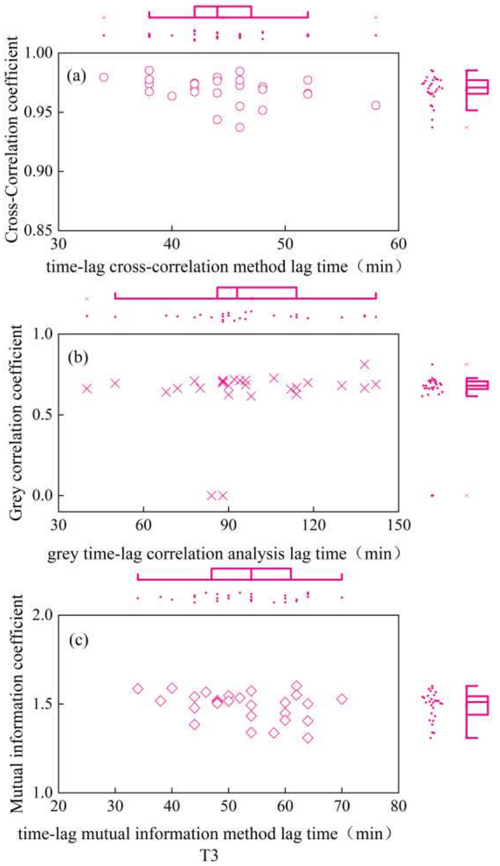

Fig. 10 Time lag parameter and corresponding coefficients for T3 calculated by time-lag cross-correlation method,time-lag mutual information method, and grey time-lag correlation analysis

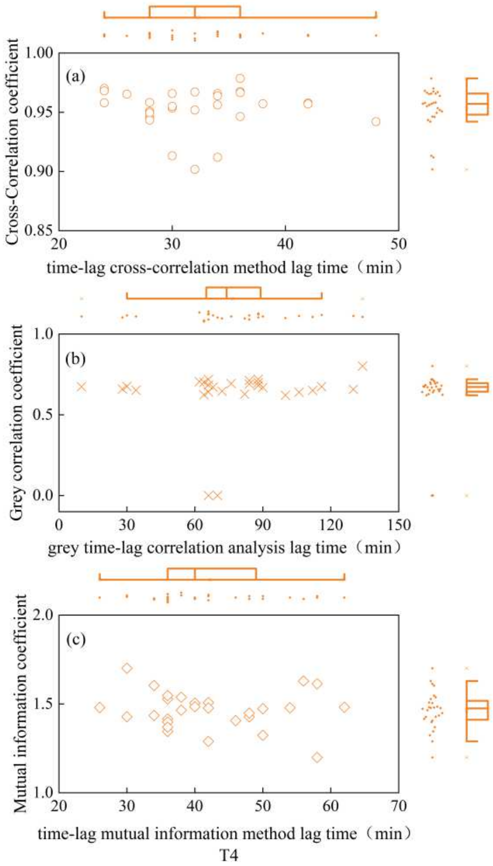

Fig. 11 Time lag parameter and corresponding coefficients for T4 calculated by time-lag cross-correlation method,time-lag mutual information method, and grey time-lag correlation analysis

Accuracy of CWSI inversion of Pn, Tr and gs before and after correction for time lag

Time-lag peak-seeking method, time-lag cross-correlation method,time-lag mutual information method, and grey time-lag correlation analysis

As shown in Figs. 12, 13, correcting the time lag between Ta and Tc improved the accuracy of CWSI inversion for Pn. After CWSI empirical and theoretical models were corrected using the time-lag peak-seeking method, time-lag cross-correlation method, time-lag mutual information method, and grey time-lag correlation analysis, the correlation between CWSI and Pn improved for all methods, with the empirical model showing more significant improvement. This indicated that time lag effect had a substantial impact on the accuracy of CWSI empirical model in inverting Pn, while its impact on the accuracy of CWSI theoretical model in inverting Pn was small and negligible.

As shown in Figs. 14,15, the time lag effect has a small impact on the accuracy of CWSI theoretical model inverting Tr and a large impact on the accuracy of the CWSI empirical model inverting Tr; The correlation between CWSI and Tr does not change after correcting CWSI theoretical model by using the time-lag peak-seeking method; The correlation between CWSI and Tr is improved by correcting CWSI theoretical model,with using time-lag cross-correlation method,time-lag mutual information method, and grey time-lag correlation analysis; The correlation between Tr and the CWSI theoretical model corrected based on grey time-lag correlation analysis and time-lag mutual information is the best ($R^2 = 0.90$). The correlation between CWSI empirical model and Tr decreases after correcting CWSI empirical model using the time-lag mutual information method and grey time-lag correlation analysis; The accuracy of CWSI inversion of Tr improves after correcting CWSI empirical model using the time-lag peak-seeking method and time-lag mutual correlation method; The correlation between Tr and CWSI empirical model corrected based on the time-lag mutual correlation method is the highest ($R^2 = 0.94$).

As demonstrated in Figs. 16,17, the correlation between CWSI and gs remained unchanged after CWSI theoretical model was corrected by applying the time-lag peak-seeking method. However, the correlation between CWSI and gs improved after CWSI theoretical model was corrected using the time-lag cross-correlation method, the time-lag mutual information method, and the grey time-lag correlation analysis. Notably, the time-lag mutual information method enhanced the accuracy of the CWSI theoretical model inversion of gs the most ($R^2 = 0.96$). Time lag effect significantly impacted the accuracy of CWSI empirical model inversion of gs. The correlation between CWSI and gs increased after correcting CWSI empirical model using the time-lag peak-seeking method, the time-lag mutual correlation method, the time-lag mutual information method, and the grey time-lag correlation analysis. gs showed the highest correlation with CWSI empirical model based on the time-lag mutual information method (R^2= 0.96).

In summary, it was observed that time lag effect between Ta and Tc caused a significant impact on the accuracy of CWSI inversion of photosynthetic parameters. The impact was more substantial on the accuracy of CWSI empirical model for inverting photosynthetic parameters, and the time-lag-corrected CWSI empirical model demonstrated a higher correlation with the photosynthetic parameters. This indicated that CWSI empirical model was more sensitive to the time lag effect than CWSI theoretical model. The reason for this phenomenon might be that CWSI theoretical model required measurements of net radiation, soil heat flux, wind speed, and canopy resistance, making the theoretical models less volatile (Stockle and Dugas 1992). The correlation of the time-lag-corrected CWSI with Pn, Tr, and gs was in the order of gs>Tr>Pn. Pn showed the highest correlation with empirical/theoretical CWSI model corrected by the time-lag mutual information method (R^2=0.8); Tr had the best correlation with CWSI empirical model corrected by the time-lag mutual information method (R^2=0.93); gs exhibited the best correlation with CWSI empirical model corrected by the time-lag mutual information method (R^2=0.93). Occasionally, time-lag correction reduced the accuracy of CWSI inversion of photosynthetic parameters. This reduction could be attributed to the fact that the time lag effect between Tc and environmental factors, such as relative humidity and solar radiation, was not accounted for (Ricotta et al. 1997).

Meanwhile, time lag effect was the result of the continuous direct or indirect influence of previous environmental factors on crops, representing an accumulative process (Ding et al. 2020; He et al. 2024; Xu et al. 2023). Time-lag peak-finding method, which utilized a function to fit the daily change curve of Tc and Ta and defined the time lag parameter solely by the time difference between its peak points, exhibited certain limitations.

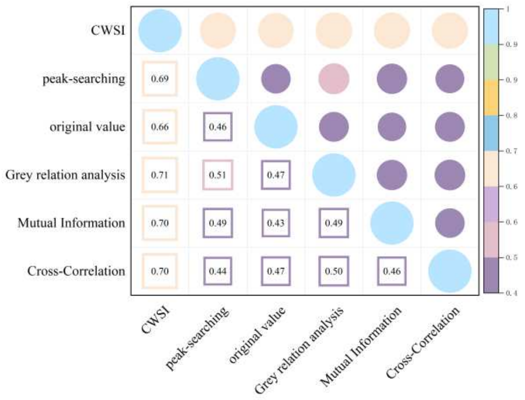

Fig. 12 Heat map of CWSI theoretical model of before and after correction of the time lag with Pn

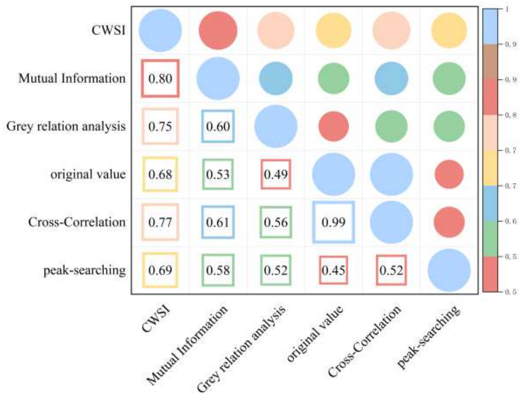

Fig. 13 Heat map of CWSI experience model of before and after correction of the time lag with Pn

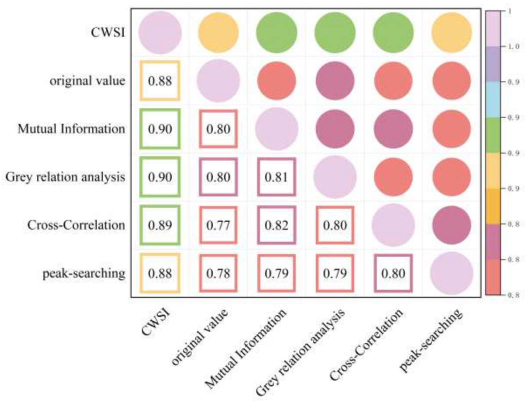

Fig. 14 Heat map of CWSI theoretical model of before and after correction of the time lag with Tr

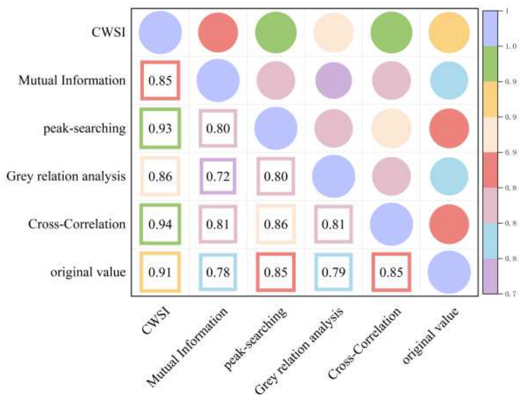

Fig. 15 Heat map of CWSI experience model of before and after correction of the time lag with Tr

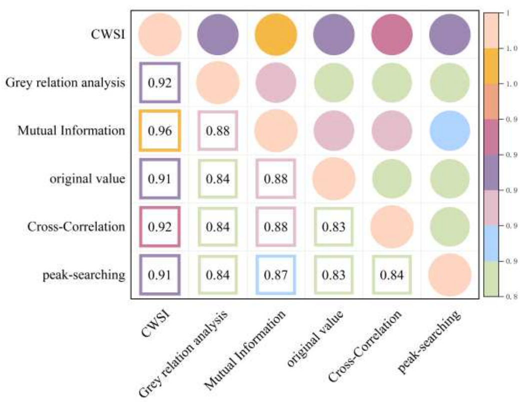

Fig. 16 Heat map of CWSI theoretical model of

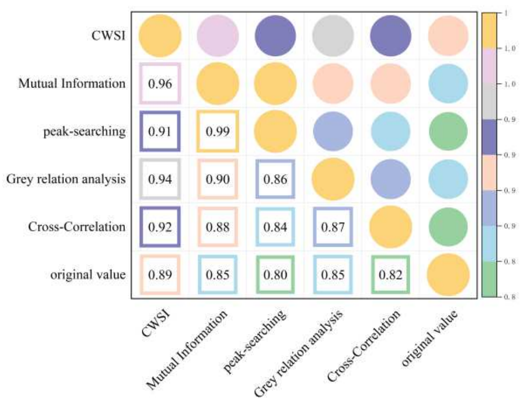

Fig. 17 Heat map of CWSI experience model of

before and after correction of the time lag with gs before and after correction of the time lag with gs

Machine learning algorithms for predicting CWSI empirical models based on time-lag mutual information correction

The accuracy of CWSI empirical model corrected based on the time-lag mutual information method for inversion of photosynthetic parameters was overall high. It was investigated by using Genetic Algorithm Optimised Support Vector Machines based on Genetic Algorithms (GA-SVM), Bayesian Optimised Long and Short-Term Memory Neural Networks (Bayes-LSTM), Particle Swarm Algorithm Optimised Long and Short-Term Memory based on Particle Swarm Algorithms (PSO-LSTM), Convolutional Bi-directional Long and Short-Term Memory Neural Networks (CNN-BILSTM), Attention Mechanism Long Short-Term Memory Neural Network (attention-LSTM), and Attention Mechanism Gated Recurrent Unit (attention-GRU) machine learning algorithms for prediction. The prediction accuracies were shown in Table 4.

with GA-SVM>Bayes-LSTM>PSO-LSTM>CNN-BILSTM>attention-LSTM>GRU-attention. The prediction accuracy of the above models for CWSI empirical model corrected by the time-lag mutual information method was higher overall. Predicted effect diagrams were showed in Fig. 18-29. GA-SVM model had the highest prediction accuracy (R^2=0.982, RMSE=0.017).

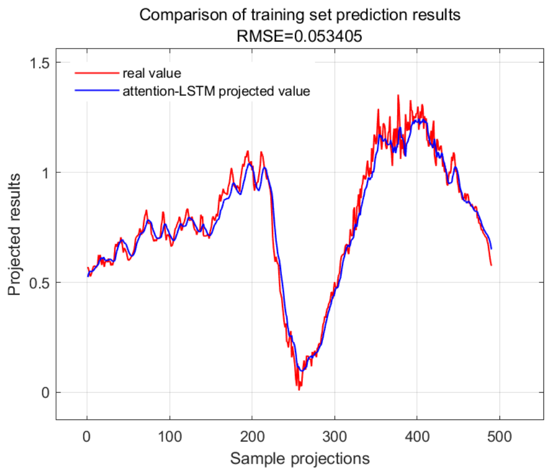

Fig. 18 Training set for attention-LSTM

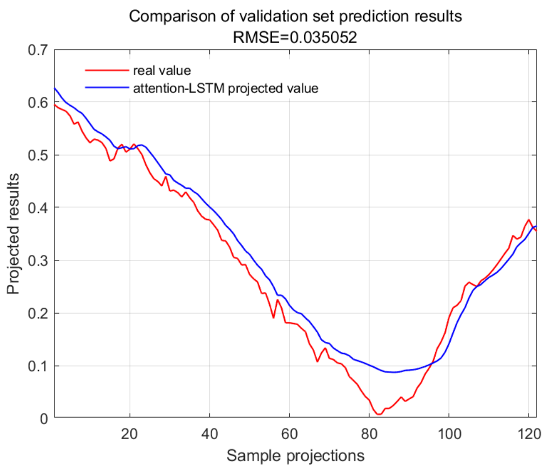

Fig. 19 Validation set for attention-LSTM

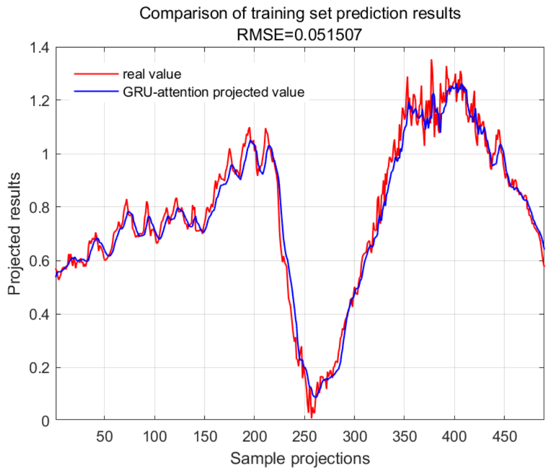

Fig. 20 Training set for GRU-attention

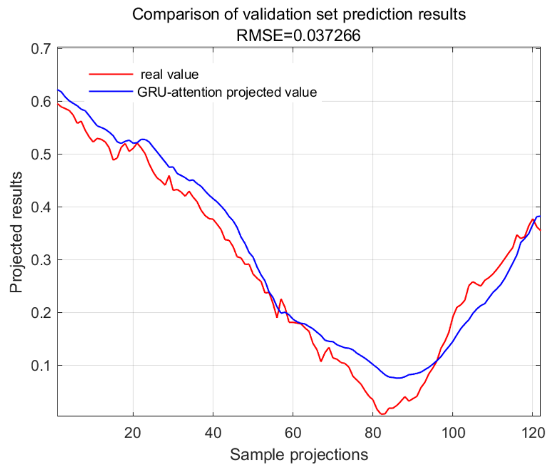

Fig. 21 Validation set for GRU-attention

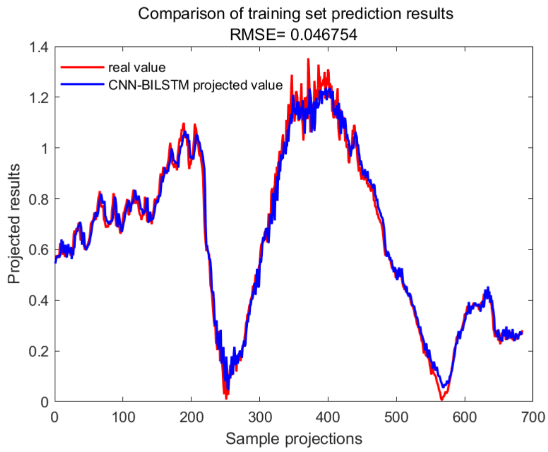

Fig. 22 Training set for CNN-BILSTM

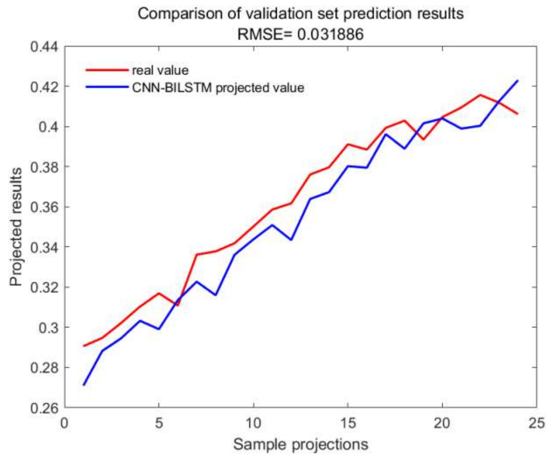

Fig. 23 Validation set for CNN-BILSTM

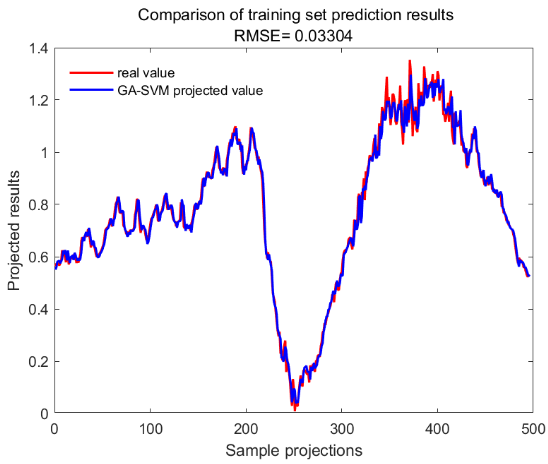

Fig. 24 Training set for GA-SVM

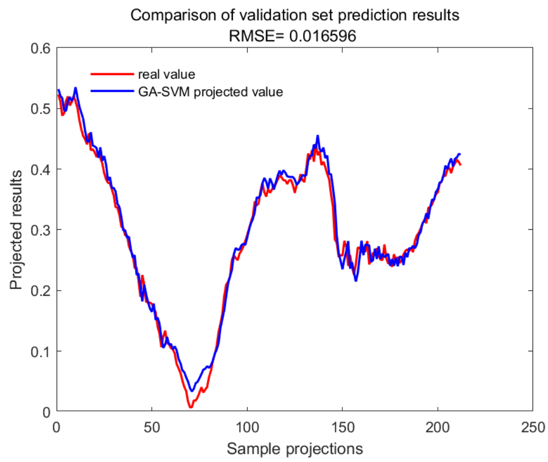

Fig. 25 Validation set for GA-SVM

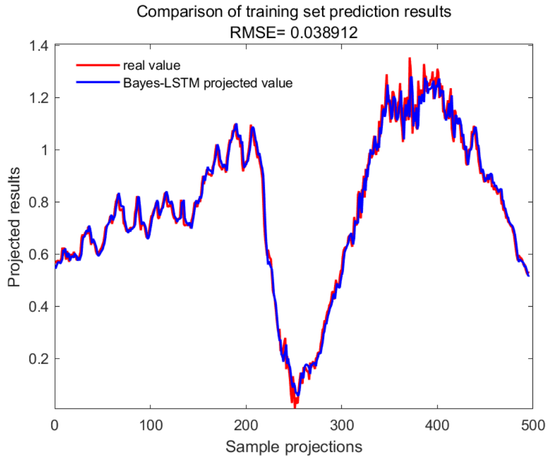

Fig. 26 Training set for Bayes-LSTM

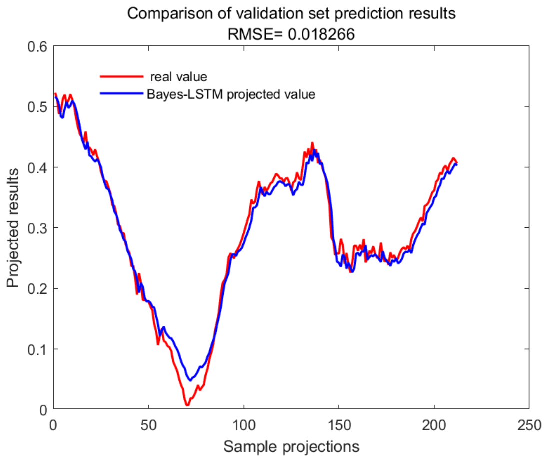

Fig. 27 Validation set for Bayes-LSTM

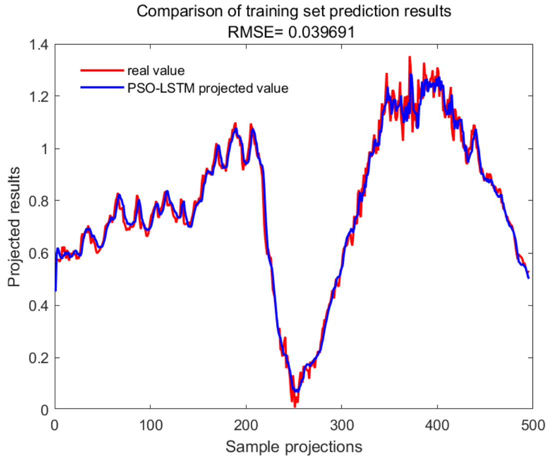

Fig. 28 Training set for PSO-LSTM

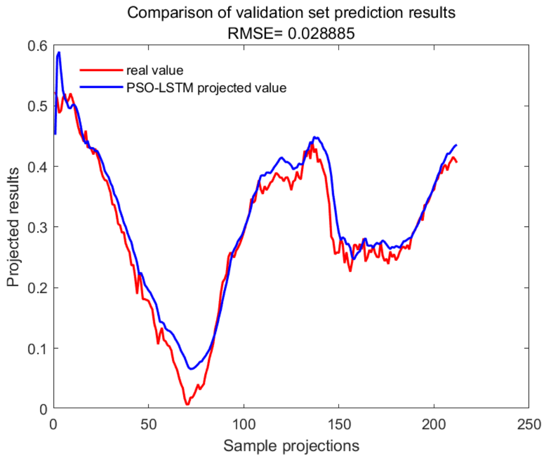

Fig. 29 Validation set for PSO-LSTM

Table 4 Prediction accuracy of machine learning algorithms for CWSI empirical models based on time-lag mutual information correction

Machine Learning Algorithm	R^2	RMSE
attention-LSTM	0 .88928	0.035052
GRU-attention	0.80197	0.037266
CNN-BILSTM	0.9148	0.031886
GA-SVM	0.98237	0.016596
PSO-LSTM	0.9466	0.028885
Bayes-LSTM	0.97865	0.018266

Discussions

Time lag parameters between Tc and Ta calculated by different models

The essence of the peak-finding method is to find a suitable function for fitting (Mukoyama 2017), and the time difference of the peak of the curve is the time lag parameter between the two series. In this study, CCE equation was applied to fit Tc of winter wheat after S-G filter smoothing, and ECS equation was applied to fit Ta after S-G filter smoothing. This is in general agreement with the time lag parameter of Tc and Ta for summer maize obtained by Zhang et al. (2022). Considering that the time lag effect was the persistent influence of previous climatic conditions on current crop growth as a result of the cumulative effects of meteorological factors and soil moisture content on the crop (Braswell et al. 1997; Ma et al. 2022), there were limitations in determining the time lag parameter through isolated points.Therefore, the time lag parameter between Ta and Tc was calculated using the time-lag cross-correlation method (Pallotta and Giunta 2022). The time lag parameter calculated in this study was about 32-44 minutes, consistent with the findings of Zhang Z et al. (2023).

Meanwhile, this study innovatively utilized the time-lag mutual information method (Albers and Hripcsak 2012) and grey time-lag correlation analysis (Liu et al. 2022) to calculate the time lag parameter between Ta and Tc. The time lag parameter calculated by the time-lag mutual information method ranged from 42 to 58 min, while the grey time-lag correlation analysis calculated time lag parameter ranged from 42 to 58 min76 to 98 min. Additionally, the time lag parameter between Tc and Ta in winter wheat calculated by the four methods all experienced a significant sudden drop under the heavy water stress treatment. Pn, Tr, and gs all exhibited a decreasing trend with diminishing soil moisture (Liu et al. 2023), and a sudden drop occurred in the heavy water stress treatment (T4) (Liu EK et al. 2016). This phenomenon might be related to the soil moisture quench value (Carrasco-Benavides et al. 2024).

Mild water stress does not affect the normal life activities of the crop, and the physiological activities of the plant are limited only when the degree of drought stress exceeds the drought threshold. When the soil moisture threshold is reached, stomata are reduced or closed, and water lost through stomatal transpiration and CO_2 entering the chloroplasts are reduced (Egan et al. 2021). As a result, Pn, Tr, and gs undergo varying degrees of reduction (Didion-Gency et al. 2022).Wu et al. (2000) found that when the soil volumetric water content was lower than 60% of field holding capacity for a long period of time, the leaf enlargement was restricted, the total leaf area for light energy interception was reduced, and the gas exchange process of winter wheat was limited, which was the reason for the sudden decrease of photosynthetic parameters under severe water stress. At the same time, the decrease in stomatal conductance reduces crop transpiration, evaporative cooling was reduced, and canopy temperatures continue to rise (Struthers et al. 2015), reaching their peaks later, resulting in a decrease in the time lag parameter between Tc and Ta in the heavy water stress treatment. Liu et al. (2003) found that the soil moisture queue value of winter wheat was about 43.5%-52.2% of the soil water content, which was consistent with the soil moisture treatments in this experiment in which there were abrupt changes in photosynthetic and time-lag parameters.

Reasons for different changes in the magnitude of the accuracy of the CWSI inversions Pn, Tr, and gs before and after correction of the time lag

After considering the time-lag effect, the magnitudes of correlations between CWSI and Pn, Tr, and gs varied inconsistently, which might be related to the different major environmental factors affecting Pn, Tr, and gs (Maai et al. 2020), as well as their distinct critical soil moisture thresholds. When the crop was not subjected to water stress, environmental factors had a small and negligible effect on Pn, Tr was mainly limited by solar radiation, and gs was primarily limited by photosynthetically active radiation and crop canopy temperature. When crops were subjected to water stress, Pn was mainly limited by relative humidity and atmospheric temperature, Tr was chiefly limited by saturated water-vapour pressure difference, and gs was predominantly limited by saturated water-vapour pressure difference and wind speed (Zhou et al. 2022). Meanwhile, Pn, Tr, and gs showed different sensitivities to soil water deficit. The critical soil moisture thresholds for Pn, Tr, and gs were 62%, 60%, and 58% for maize at the seedling stage and 51%, 53%, and 48% at the nodulation stage. This indicated that crop photosynthetic parameters were sensitive to soil moisture in the order of gs>Tr>Pn, consistent with the magnitude of CWSI correlation with Pn, Tr, and gs obtained in this study (Ma et al. 2018). At the same time, this might result in a varying degree of improvement in the correlation between CWSI and Pn, Tr, and gs before and after accounting for time lag effect (gs>Tr>Pn).

Outlook

Physiological parameters of plants at different growth stages exhibit varying sensitivities to soil moisture (Ma et al. 2024). This suggests that the photosynthetic parameters of winter wheat at different fertility stages show differential sensitivities to CWSI under varying water stress conditions. The impact of water stress on the crop's gas exchange processes is minimal during the regrowth period, with little variation in Pn, Tr, and Gs across different water stress levels. However, the inhibitory effects of persistent water stress during the nodulation-irrigation period are more pronounced, indicating a more significant decrease in Pn, Tr, and gs in winter wheat under severe water stress (Zhao et al. 2020) . Therefore, there are significant seasonal variations in the correlation of CWSI with Pn, Tr, and gs in winter wheat subjected to different moisture treatments. In this study, the impact of time lag effect on the accuracy of CWSI inversion of photosynthesis parameters is investigated only for the entire reproductive period. The influence of time lag between Ta and Tc on the accuracy of CWSI inversion of photosynthesis parameters during each reproductive phase is not discussed and requires further study.

Conclusions

In this study, we investigated the impact of time lag effect between Tc and Ta on the correlation between

CWSI and photosynthetic parameters.The main conclusions were as follows: (1) The magnitude of the time lag parameter between Tc and Ta in winter wheat calculated by the four methods for the whole reproductive period: grey time lag correlation analysis > time lag peak-seeking method > time lag mutual information method > time lag mutual correlation method, and all of the time lag parameters of the heavy water stress treatments were subjected to a sudden decrease. (2) CWSI empirical model was more sensitive to time lag effect than CWSI theoretical model, and time-lag correction improved the accuracy of CWSI inversion of photosynthetic parameters. CWSI corrected based on the time-lag mutual information method correlated better overall with photosynthetic parameters. Pn had the highest correlation with CWSI empirical model after correction based on the time-lag mutual information method (R^2 = 0.8);Tr had the highest correlation with empirical CWSI model after correction based on the time-lag cross-correlation method (R^2=0.93);gs had the highest correlation with the corrected CWSI empirical/theoretical model based on the time-lag mutual information approach (R^2=0.96); (3) Accuracy of machine learning algorithms for predicting daily change processes in CWSI empirical model corrected based on the time-lag mutual information method:

GA-SVM>Bayes-LSTM>PSO-LSTM>CNN-BILSTM>attention-LSTM>GRU-attention.GA-SVM had the highest prediction accuracy (R^2 = 0.982, RMSE = 0.017).

Statements & Declarations

Funding

This study was fnancially supported by the National Natural Science Foundation of China (51979232, 52179044), Natural Science Foundation in Shaanxi Province of China (2019JM-066).

Competing interests

Authors guarantee that they have no financial or non-financial interests directly or indirectly related to the work submitted for publication. Author declare that they have no known competing financial interests or personal relationships that could appear to influence the work reported in this paper.

Author contributions

Yujin Wang: Field trials collecting data, analysing data, conceptualising, calculating, writing first drafts; Yule Lu: Assistance in calculating data; Ning Yang: Assisting with experiments; Junying Chen: Assistance with conceptualization; Jiankun Wang, Zugui Huang, Youzhen Xiang: Assistance in reviewing manuscripts.

References

Albers DJ, Hripcsak G (2012) Estimation of time-delayed mutual information and bias for irregularly and sparsely sampled time-series. Chaos Solitons Fractals 45:853-860. https://doi.org/10.1016/j.chaos.2012.03.003

Braswell BH, Schimel DS, Linder E, Moore B (1997) The response of global terrestrial ecosystems to interannual temperature variability. Science 278:870-873. https://doi.org/10.1126/science.278.5339.870

Cao D, Xu N, Chen Y, Zhang HY, Li YT, Yuan ZM (2022) Construction of a pearson- and MIC-based co-expression network to identify potential cancer genes. Interdiscip Sci 14:245-257. https://doi.org/10.1007/s12539-021-00485-w

Carrasco-Benavides M, Espinoza-Meza S, Umemura K, Ortega-Farías S, Baffico-Hernández A, Neira-Román J, Ávila-Sánchez C, Fuentes S (2024) Evaluation of thermal-based physiological indicators for determining water-stress thresholds in drip-irrigated ‘Regina’ cherry trees. Irrig Sci. https://doi.org/10.1007/s00271-024-00916-8

Desoky E-SM, Mansour E, El-Sobky E-SEA, Abdul-Hamid MI, Taha TF, Elakkad HA, Arnaout SMAI, Eid RSM, El-Tarabily KA, Yasin MAT (2021) Physio-Biochemical and Agronomic Responses of Faba

Beans to Exogenously Applied Nano-Silicon Under Drought Stress Conditions. Front Plant Sci 12:637783. https://doi.org/10.3389/fpls.2021.637783

Didion-Gency M, Gessler A, Buchmann N, Gisler J, Schaub M, Grossiord C (2022) Impact of warmer and drier conditions on tree photosynthetic properties and the role of species interactions. New Phytol 236:547-560. https://doi.org/10.1111/nph.18384

Ding Y, Li Z, Peng S (2020) Global analysis of time-lag and -accumulation effects of climate on vegetation growth. Int J Appl Earth Obs Geoinf 92:102179. https://doi.org/10.1016/j.jag.2020.102179

Egan L, Hofmann R, Nichols S, Hadipurnomo J, Hoyos-Villegas V (2021) Transpiration Rate of White Clover (Trifolium repens L.) Cultivars in Drying Soil. Front Plant Sci 12:595030. https://doi.org/10.3389/fpls.2021.595030

Farooq M, Kobayashi N, Ito O, Wahid A, Serraj R (2010) Broader leaves result in better performance of indica rice under drought stress. J Plant Physiol 167:1066-1075. https://doi.org/10.1016/j.jplph.2010.03.003

Feng S, Zhang Z, Zhao S, Guo X, Zhu W, Das P (2023) Time lag effect of vegetation response to seasonal precipitation in the Mara River Basin. Ecol Process 12:49. https://doi.org/10.1186/s13717-023-00461-w.

Gontia NK, Tiwari KN (2008) Development of crop water stress index of wheat crop for scheduling irrigation using infrared thermometry. Agric Water Manag 95:1144-1152. https://doi.org/10.1016/j.agwat.2008.04.017

Gonzalez-Dugo V, Zarco-Tejada PJ (2022) Assessing the impact of measurement errors in the calculation of CWSI for characterizing the water status of several crop species. Irrigation Science. https://doi.org/10.1007/s00271-022-00819-6

Guo Y, Mao H, Ding H, Wu X, Liu Y, Liu H, Zhou S (2022) Data-Driven Coordinated Development of the Digital Economy and Logistics Industry. Sustainability 14:8963. https://doi.org/10.3390/su14148963

Hatfield JL (1983) The utilization of thermal infrared radiation measurements from grain sorghum crops as a method of assessing their irrigation requirements. Irrig Sci 3:259-268. https://doi.org/10.1007/BF00272841

He X, Liu A, Tian Z, Wu L, Zhou G (2024) Response of Vegetation Phenology to Climate Change on the Tibetan Plateau Considering Time-Lag and Cumulative Effects. Remote Sensing. Remote Sens 16:49. https://doi.org/10.3390/rs16010049

Huang J, Wang S, Guo Y, Chen J, Yao Y, Chen D, Liu Q, Zhang Y, Zhang Z, Xiang Y (2022) Hysteresis between winter wheat canopy temperature and atmospheric temperature and its driving factors. Plant Soil. https://doi.org/10.1007/s11104-022-05509-y

Idso S, Jackson R, Pinter Jr P, Reginato R, Hatfield JJAm (1981) Normalizing the stress-degree-day parameter for environmental variability. Agric Meteorol 24:45-55. https://doi.org/10.1016/0002-1571(81)90032-7

Jackson RD, Idso S, Reginato R, Pinter Jr PJWrr (1981) Canopy temperature as a crop water stress indicator. Water Resour Res 17:1133-1138. https://doi.org/10.1029/WR017i004p01133

Ji C, Ma F, Wang J, Wang J, Sun W (2021) Real-Time Industrial Process Fault Diagnosis Based on Time Delayed Mutual Information Analysis. Processes 9:1027. https://doi.org/10.3390/pr9061027

Kifle M, Gebretsadikan TG (2016) Yield and water use efficiency of furrow irrigated potato under regulated deficit irrigation, Atsibi-Wemberta, North Ethiopia. Agric Water Manag 170:133-139. https://doi.org/10.1016/j.agwat.2016.01.003

Konda F, Okamura M, Ali Akbar M, Yokoi T (1996) Fiber Speed and Yarn Tension in Friction Spinning. Text Res J 66:343-348. https://doi.org/10.1177/004051759606600509

Liu C, Chen Y, Zou L, Cheng B, Huang T (2022) Time-Lag Effect: River Algal Blooms on Multiple Driving Factors. Front Earth Sci 9:813287. https://doi.org/10.3389/feart.2021.813287

Liu EK, Mei XR, Yan CR, Gong DZ, Zhang YQ (2016) Effects of water stress on photosynthetic characteristics, dry matter translocation and WUE in two winter wheat genotypes. Agric Water Manag 167:75-85. https://doi.org/10.1016/j.agwat.2015.12.026

Liu J, Wang F, Yu Q, Mao F, Bi J, Fan G (2003) Application of the leaf photosynthesis model for forecasting effect of drought on winter in north china plain. Journal of Applied Meteorological Science 14:469-478.

Liu J, Zhang J, Shi Q, Liu X, Yang Z, Han P, Li J, Wei Z, Hu T, Liu F (2023) The Interactive Effects of Deficit Irrigation and *Bacillus pumilus* Inoculation on Growth and Physiology of Tomato Plant. Plants 12:670. https://doi.org/10.3390/plants12030670

Liu YP, Dang B, Li Y, Lin H, Ma H (2016) Applications of Savitzky-Golay Filter for Seismic Random Noise Reduction. Acta Geophys 64:101-124. https://doi.org/10.1515/acgeo-2015-0062.

Ma S, Liu S, Gao Z, Wang X, Ma S, Wang S (2024) Water Deficit Diagnosis of Winter Wheat Based on Thermal Infrared Imaging. Plants 13:361. https://doi.org/10.3390/plants13030361

Ma X, He Q, Zhou G (2018) Sequence of Changes in Maize Responding to Soil Water Deficit and Related Critical Thresholds. Front Plant Sci 9:511. https://doi.org/10.3389/fpls.2018.00511

Ma Y, Guan Q, Sun Y, Zhang J, Yang L, Yang E, Li H, Du Q (2022) Three-dimensional dynamic characteristics of vegetation and its response to climatic factors in the Qilian Mountains. CATENA 208:105694. https://doi.org/10.1016/j.catena.2021.105694

Maai E, Nishimura K, Takisawa R, Nakazaki TJPPS (2020) Light stress-induced chloroplast movement and midday depression of photosynthesis in sorghum leaves. Plant Prod Sci 23:172-181. https://doi.org/10.1080/1343943X.2019.1673666

Mukoyama T (2017) Fitting of Gaussian peaks by simulated annealing. X-Ray Spectrom 46:63-68. https://doi.org/10.1002/xrs.2728

Pallotta L, Giunta G (2022) Accurate Delay Estimation for Multisensor Passive Locating Systems Exploiting the Cross-Correlation Between Signals Cross-Correlations. IEEE Trans Aerosp Electron Syst 58:2568-2576. https://doi.org/10.1109/TAES.2021.3116927

Pipatsitee P, Eiumnoh A, Praseartkul P, Taota K, Kongpugdee S, Sakulleerungroj K, Cha-um S (2018) Application of infrared thermography to assess cassava physiology under water deficit condition. Plant Prod Sci 21:398-406. https://doi.org/10.1080/1343943X.2018.1530943

Ricotta C, Avena GC, Teggi S (1997) Relation between vegetation canopy surface temperature and the Sun-surface geometry in a mountainous region of central Italy. Int J Remote Sens 18:3091-3096. https://doi.org/10.1080/014311697217251

Saini S, Raj K, Saini AK, Kumar R, Saini A, Khan A, Kumar P, Devi G, Bhambhu MK, McKenzie CL, Lal M, Wati L (2024) Unravelling the synergistic interaction of Thrips tabaci and newly recorded, Thrips parvispinus with Alternaria porri (Ellis.) Cif., inciting onion purple blotch. Front Microbiol 15:1321921. https://doi.org/10.3389/fmicb.2024.1321921

Stockle CO, Dugas WA (1992) Evaluating canopy temperature-based indices for irrigation scheduling. Irrig Sci 13:31-37. https://doi.org/10.1007/BF00190242

Struthers R, Ivanova A, Tits L, Swennen R, Coppin P (2015) Thermal infrared imaging of the temporal variability in stomatal conductance for fruit trees. Int J Appl Earth Obs Geoinf 39:9-17. https://doi.org/10.1016/j.jag.2015.02.006

Su Z-Y, Wu T, Wang Y-T, Huang H-Y (2008) An investigation into the linear and nonlinear correlation of two music walk sequences. Physica D 237:1815-1824. https://doi.org/10.1016/j.physd.2008.01.029

Wang Y, Huang Y, Zeng X, Wei G, Zhou J, Fang T, Chen H (2017) Faulty Feeder Detection of Single Phase-Earth Fault Using Grey Relation Degree in Resonant Grounding System. IEEE Trans Power Deliv 32: 55-61. https://doi.org/10.1109/TPWRD.2016.2601075

Wu H, Duan A, Yang C (2000) Physiological and Morphological Responses of Winter Wheat to Soil Moisture. Acta Agriculturae Boreali-Sinica 15:92-96.

Xu S, Wang Y, Liu Y, Li J, Qian K, Yang X, Ma X (2023) Evaluating the cumulative and time-lag effects of vegetation response to drought in Central Asia under changing environments. J Hydrol 627:130455. https://doi.org/10.1016/j.jhydrol.2023.130455

Yuan G, Luo Y, Tang D, Yu Q, Yu L (2002) Estimating Minimum Canopy Resistances of Winter Wheat at Different Development Stages. Acta Ecologica Sinica 6:930-934.

Zeng C, Lai W, Lin H, Liu G, Qin B, Kang Q, Feng X, Yu Y, Gu R, Wu J, Mao L (2023) Weak information extraction of gamma spectrum based on a two-dimensional wavelet transform. Radiat Phys Chem 208:110914. https://doi.org/10.1016/j.radphyschem.2023.110914

Zhang M, Chen W, Jing M, Gao Y, Wang Z (2023) Canopy Structure, Light Intensity, Temperature and Photosynthetic Performance of Winter Wheat under Different Irrigation Conditions. Plants 12:3482. https://doi.org/10.3390/plants12193482

Zhang Q, Yang X, Liu C, Yang N, Yu G, Zhang Z, Chen Y, Yao Y, Hu X (2024) Monitoring soil moisture in winter wheat with crop water stress index based on canopy-air temperature time lag effect. Int J Biometeorol 68:647-659. https://doi.org/10.1007/s00484-023-02612-2

Zhang Z, Wu T, Yu G, Bai X, Zhang Y, Huang J (2022) Time delay effect of summer maize canopy temperature change and its influence on soil moisture content monitoring. Nongye Gongcheng Xuebao 38:117-124. https://doi.org/10.11975/j.issn.1002-6819.2022.01.013.

Zhang Z, Zhang Q, Yang N, Luo L, Huang J, Yao Y (2023) Time Lag Effect between Winter Wheat Canopy Temperature and Atmospheric Temperature and Its Influencing Factors. Nongye Jixie Xuebao 54:359-368. https://doi.org/10.6041/j.issn.1000-1298.2023.11.034.

Zhao W, Liu L, Shen Q, Yang J, Han X, Tian F, Wu J (2020) Effects of Water Stress on Photosynthesis, Yield, and Water Use Efficiency in Winter Wheat. Water 12:2127. https://doi.org/10.3390/w12082127

Zhou P, Gao P, Chen W, Yang M, Ding Z, Liu H, Wang W (2022) Response of photosynthetic parameters of citrus trees to water and meteorological factors under different water treatments. Water Saving Irrigation 6:90-95.